Prostate Brachytherapy Seed Localization with Gaussian Blurring and Camera Self-calibration[*]

Junghoon Lee[1], Xiaofeng Liu[2], Jerry L. Prince[1], and Gabor Fichtinger[2,3]

[1] Department of Electrical and Computer Engineering and
[2] Computer Science, Johns Hopkins University, Baltimore, MD USA
[3] School of Computing, Queen's University, Canada

Abstract. A tomosynthesis-based prostate brachytherapy seed localization method is described. Gaussian-blurred images are computed from a limited number of X-ray images, and a 3-D volume is reconstructed by backprojection. Candidate seed locations are extracted from the reconstructed volume and false positive seeds are removed by optimizing a local cost function. In case where the estimated pose error is large, a self-calibration process corrects the estimation error of the intrinsic camera parameters and the translation of the pose in order to improve the reconstruction. Simulation and phantom experiment results imply that the implanted seed locations can be estimated from four or five images depending on the number of seeds. The algorithm was also validated using patient data, successfully localizing the implanted seeds.

1 Introduction

Prostate cancer is one of the leading cancers in men in North America and brachytherapy is a definitive treatment for low risk prostate cancer, which involves permanent implantation of radioactive seeds into the prostate. Its success mainly depends on the ability to treat the target gland with a sufficient amount of therapeutic dose while sparing adjacent healthy organs from excessive radiation. Even if a preoperative implantation plan is made based on idealistic seed patterns and an ultrasound volume study, errors are usually introduced during the actual implantation procedure due to various reasons e.g. patient motion, deviation of the needle, and edema. In order to overcome these limitations, intraoperative planning under the guidance of ultrasound and fluoroscopy was proposed.

There are various approaches to localize brachytherapy seeds from a limited number of X-ray images. There are correspondence-based methods which solve seed matching problems between identified seeds in different images [1, 2, 3, 4, 5, 6, 7]. These methods require accurate identification of the seeds in all images because incorrect localization of the seeds will cause undetected seeds in 3-D reconstruction. However, it is hard to perfectly identify the seeds in all images, since typically up to 7% of the seeds can be hidden in the X-ray images [6]. The

---

unidentified seeds are usually recovered manually and sometimes requires extra X-ray images, which is time consuming. It is sometimes impossible to recover them when seeds are completely hidden in some unsuspected constellation.

Tutar *et al.* [8] proposed a selective backprojection method which is a modified tomosynthesis technique. However their seed detection and false positive (FP) seed removal process is very sensitive to the C-arm pose estimation errors since their detection process is based on the detected seed size. A tomosynthesis algorithm based on a distance map was previously developed [9] to compensate for the pose estimation errors. However, sometimes the reconstruction is severely deteriorated when any of the estimated C-arm poses has relatively large errors.

In order to make the reconstruction robust to the C-arm pose and calibration errors, a self-calibration process using candidate seeds detected from an initial reconstruction based on the Gaussian-blurred images is introduced.

2   Methods

2.1   Image Acquisition, Calibration and Gaussian Blurring

X-ray projection images are acquired from a C-arm within a limited angle, e.g. $\leq$ 20° due to the limited space in the operating room near the patient. Each image is calibrated and its geometric distortion is corrected by the parameters previously computed from calibration phantom images. For each image, the pose of the C-arm is computed using a fluoroscope tracking (FTRAC) fiducial originally developed by Jain *et al.* with an estimation accuracy of 0.56 mm in translation and 0.33° in orientation [10].

Since the background is highly nonuniform in actual patient images and the size of the seeds are very small, the nonuniform background can be extracted by dilation and is subtracted from the original distortion-corrected image. The seed cloud region in each image is selected by semi-automated morphological operators and binary seed-only images are computed from the background-subtracted images by adaptive thresholding. Euclidean distance between each pixel and its nearest seed region is computed by distance transform and an unnormalized Gaussian-blurred image is computed by the following equation.

$$I(\mathbf{x}) = \exp\left[-\frac{d(\mathbf{x})^2}{2\sigma^2}\right] \tag{1}$$

where $I(\cdot)$ is the Gaussian-blurred image, $\mathbf{x} \in \mathrm{R}^2$ is the pixel location in the image, d is the distance map of the image, and σ^2 is the variance which controls the blur width. Since we do not need to identify all seeds in the 2-D images, overlapping seeds are simultaneously considered to be at zero distance. The pixel value inside the seed regions is 1 and the pixel value tapers down as the distance between the pixel and the nearest seed region increases. σ^2 is determined depending on the size of the seeds and the pose estimation errors. The fundamental idea of this approach is that a pixel closer to the seed region in the seed-only image has higher probability that it belongs to the true seed region, while a pixel farther from the seed regions has lower probability of belonging to the true seed region.

2.2   Volume Reconstruction and Candidate Seeds Detection

Projection matrices are first computed for both reconstruction and cost computation for FP seeds removal based on the intrinsic camera parameters computed by the calibration phantom and the extrinsic camera pose of the C-arm computed by the FTRAC, and then a 3-D volume is reconstructed using backprojection, which is equivalent to a generalized form of tomosynthesis for arbitrary orientations. Since the reconstructed voxels take values between 0 to 1 due to the nature of the Gaussian-blurred images, candidate seed regions can be extracted by thresholding. The threshold varies within a small range, e.g. 0.9–1.0, thus making the automatic thresholding possible. The extracted seed regions are labeled using connected component labeling. Each labeled seed region is considered as a candidate seed and its centroid is computed by averaging the 3-D coordinates of the voxels in that region.

2.3   Camera Self-calibration Using Detected Candidate Seeds

Gaussian blurring makes the algorithm more robust to the C-arm pose estimation errors than other tomosynthesis-based approaches. However, it is often necessary to correct the estimated pose especially when the estimation errors are large. Large errors in pose estimation easily deteriorate the reconstruction and lower the candidate seed detectability.

In general, the focal length and the origin of the image are computed using the calibration phantom prior to the operation, and the pose of the C-arm at each pose is estimated by the tracking system (in our case, the FTRAC system). However, the focal length and the origin of the image vary as the pose of the C-arm changes, which causes errors in the pose estimation. Through various simulations, the orientation estimation of the FTRAC was robust, but the translation estimation was a little sensitive to these variations [10, Sec. III]. Thus if a residual error of the pose estimation is relatively large, re-calibration and pose correction (especially for translational error correction) are required to improve the reconstruction. The incorrectly estimated intrinsic camera parameters and the pose of the C-arm can be automatically adjusted based on the Gaussian-blurred images and the candidate seeds detected from images whose corresponding C-arm poses are relatively well estimated.

Let $^S\mathbf{R}_F$ and $^S\mathbf{t}_F$ be a rotation matrix and a translation vector, respectively, from a global reference coordinates (F) to the source coordinates (S) estimated from a tracking system, and f and (o_x, o_y) be a focal length and an origin of each image, respectively, estimated by the calibration phantom. Then a 3×4 projection matrix, $^I\mathbf{F}_F$, from a global reference coordinates (F) to an image coordinates (I) can be computed by

$$^I\mathbf{F}_F = \begin{bmatrix} -\frac{f+\Delta f}{S_x} & 0 & o_x + \frac{\Delta o_x}{S_x} & 0 \\ 0 & -\frac{f+\Delta f}{S_y} & o_y + \frac{\Delta o_y}{S_y} & 0 \\ 0 & 0 & 1 & 0 \end{bmatrix} \begin{bmatrix} ^S\mathbf{R}_F & ^S\mathbf{t}_F + \Delta\mathbf{t} \\ \mathbf{0}^T & 1 \end{bmatrix} \tag{2}$$

where Δf is a focal length estimation error and $(\Delta o_x, \Delta o_y)$ is an origin of image estimation error, S_x and S_y are pixel sampling intervals along the x and y axes, respectively, and $\Delta \mathbf{t} = (\Delta t_x, \Delta t_y, \Delta t_z)^T$ is a translation estimation error.

From Eqs. (1) and (2), the unknown parameters can be estimated by solving a following optimization problem.

$$\hat{e} = \arg \min_{e} \left[-\sum_{j=1}^{N_c} I_i \left({}^I\mathbf{F}_F(e)\mathbf{x}_j \right) \right] \tag{3}$$

where N_c is the number of candidate seeds used, $\mathbf{x}_j$ is the homogeneous coordinates of the jth candidate seed, $I_i(\cdot)$ is the ith Gaussian-blurred image computed by Eq. (1), $e = (\Delta \mathbf{t}, \Delta f, \Delta o_x, \Delta o_y)$ is a nuisance parameter and $\hat{e}$ is its estimate. Since the intrinsic camera parameters and the pose of the C-arm are initially estimated by the calibration phantom and the FTRAC fiducial, we first start from zero initial condition and solve the constrained optimization within limited search range. The upper and lower bounds can be determined considering the intrinsic calibration and the pose estimation error range. We solve this constrained optimization problem using sequential quadratic programming (SQP) with the Hessian approximation by the BFGS method [11].

2.4   False Positive Seed Removal

Since only a limited number of projection images are used for a reconstruction, a tomosynthesis-based approach is prone to introduce undesired FP seeds. Thus is necessary an FP seed elimination process from the candidate seeds. This problem is solved as an optimal geometric coverage problem as was done in [9], and the FP seeds removal process can be summarized as follows.

The goal in this process is to find the N_t true seeds from N_c candidate seeds such that all the 2-D seed regions are covered in all projection images. An FP seed is projected close to some true seeds if the image contributes to create that FP seed or far away from the seed regions if the image contributes nothing for that FP seed creation, but true seeds are not always projected close to the other true seeds. Therefore, a cost function of a given seed can be defined as a function of the sum of the closest distances between the projections of this seed and the projections of all the other true seeds, and the distance between the projection of this seed and the nearest seed region in all images. Based on this idea, a local cost function is defined as:

$$C(x_n) = -\sum_{i=1}^{N_p} \frac{1 + D^i(x_n)}{1 + d_n^i}, \text{ for all } x_n \in (\mathbf{S} - \mathbf{G}) \tag{4}$$

$$D^i(x_n) = \min_{m \neq n} ||P^i x_n - P^i x_m||, \text{ for } x_m \in \mathbf{S}$$

where $\mathbf{S}$ is a set of candidate seeds, $\mathbf{G}$ is a set of candidate seeds only by which a seed region in an image is covered (these seeds are classified as true otherwise corresponding seed regions cannot be covered), P^i is a projection matrix for the

i^{th} image, and d_n^i is the distance from the projection of x_n to the nearest seed region in the ith image. This problem is solved using greedy search iteratively. During each iteration, a seed that has the largest cost value computed by Eq. (4) is removed from **S** and **G** is updated at each iteration if there are additional seeds that cover some seed regions alone after removing one FP seed. Iteration continues until N_t seeds are left.

3   Numerical Results

Simulation studies based on synthetic projection images to evaluate the Gaussian blurred image-based method has been performed and the results were reported in [12]. The simulation results indicate that the implanted seeds can be localized with a detection accuracy of $> 98.3\%$ and $> 99.6\%$ using three and four images, respectively, up to 112 seeds when there is no pose estimation error. In this section, the proposed method based on the Gaussian blurred images and the camera self-calibration is further evaluated using phantom and clinical patient data.

3.1   Phantom Experiments

Phantom experiments were performed on a precisely fabricated seed phantom assuring ground truth for reconstruction [5, Sec. III-C]. The FTRAC was precisely attached to the phantom in a known position so that the C-arm pose can be estimated. Five data sets were generated with the numbers of seeds of 42, 57, 72, 87, and 102 keeping seed density constant at about 1.56 seeds/cc for all five data sets. For each data set, six images were acquired within a 20° cone around the AP axis using a *Philips Integris V3000* fluoroscope and were dewarped and calibrated. Five and six images selected among the six available images in each data set based on the residual pose estimation errors provided by the FTRAC software were used for 3-D reconstructions. The voxel size of the 3-D reconstructions was $0.5 \times 0.5 \times 0.5$ mm^3, and the $\sigma = 3$ pixels $= 1.5$ mm. The volume was first reconstructed without camera self-calibration process. Since the radio-opaque size of the seeds are approximately 3 times larger than the seeds used for patients, the reconstruction does not be affected so much by the pose estimation errors and the reconstruction from Gaussian blurred images without camera self-calibration works quite well. For larger number of seeds (87, 102), the reconstruction was refined by the camera self-calibration process based on candidate seeds detected using three images with smallest pose errors. The estimated seed positions were compared to the ground truth, and the results are shown in Table 1. The results imply that the implanted seed locations can be estimated with a detection accuracy of $> 97.7\%$ from five projection images.

3.2   Clinical Experiments

The proposed method was applied to three clinical patient data sets. Each data set has three different batches with different number of implanted seeds.

Table 1. Phantom experiment results

Num of seeds	Self calibration	Num of images	Number of seeds candidate	Number of seeds correctly detected	Mean ± STD error (mm)
42	no	5	42	42 (100%)	1.26 ± 0.52
		6	42	42 (100%)	1.05 ± 0.42
57	no	5	58	57 (100%)	0.77 ± 0.59
		6	57	56 (98.3%)	0.84 ± 0.47
72	no	5	72	72 (100%)	0.67 ± 0.41
		6	72	72 (100%)	0.65 ± 0.37
87	no	5	96	84 (96.6%)	0.58 ± 0.41
		6	95	85 (97.7%)	0.64 ± 0.38
	yes	5	94	85 (97.7%)	0.66 ± 0.41
		6	92	86 (98.6%)	0.77 ± 0.36
102	no	5	112	99 (97.1%)	1.49 ± 0.45
		6	107	99 (97.1%)	0.97 ± 0.50
	yes	5	106	100 (98.0%)	1.20 ± 0.41
		6	103	101 (99.0%)	1.15 ± 0.31

X-ray images were taken within a $10°$ cone around the AP axis using *OEC 9800* fluoroscope, and were first dewarped and calibrated. The FTRAC from which the pose of the C-arm at each image was estimated was precisely attached to the needle insertion template in a known position. Various number of ^{103}Pd seeds with a length of 4.92 mm and a radius of 1.0 mm (radio-opaque size of about 1.45 and 0.8 mm) were implanted into the prostates. Since it is harder to detect smaller objects in the reconstruction under the pose estimation errors, seeds are undetected due to their small radio-opaque size when images with relatively large pose estimation error are used for the reconstruction. Therefore, the camera self-calibration process becomes critical and can improve the seed detectability when pose errors are large. Based on the residual pose estimation errors computed by the FTRAC software, five images with smallest errors were selected. Three images were first used for the first reconstruction, from which candidate seeds were extracted. Self-calibration was performed for the rest two images and the re-calibrated images were added for the second reconstruction. The reconstruction voxel size was $0.5 \times 0.5 \times 0.5$ mm^3, and the σ was 5 pixels = 2.5 mm and 3 pixels = 1.5 mm for the first and the second reconstructions, respectively. Since the exact locations of the seeds were unknown, the correspondences between the projection of the estimated seeds and the actual seeds in the images were visually assessed. The estimated seed locations were also compared with those computed by an existing correspondence-based method, MARSHAL [5] and the differences were computed (Note that the advantage of our method over correspondence-based methods is described in detail in Sec. 1). The results are shown in Table 2, and an example patient image and magnified images onto which the centroids of the estimated seeds are projected are shown in Fig. 1. Since the patient images were acquired from a very small angle separation compared to the simulation and the phantom images, the algorithm sometimes suffers difficulties in localizing seeds especially in the dense seed area (e.g. patient 3).
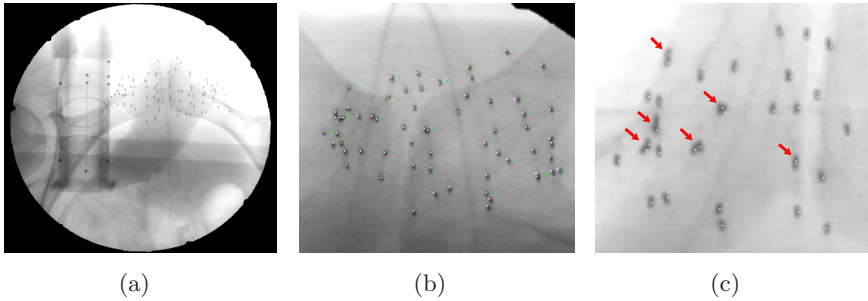
<center>(a)   (b)   (c)</center>

Fig. 1. (a) Example patient image showing 77 seeds and the FTRAC. (b) Estimated seed centroids projected onto one of the images used for reconstruction before (green dots) and after the camera self-calibration (white dots). (c) Estimated seed centroids projected onto one of the projection images used for reconstruction. Red arrows indicate hidden seeds.

<center>

Table 2. Clinical experiment results

</center>

Patient	Number of seeds			Mean ± STD
number	implanted	candidate	matched	difference (mm)
1	33	33	33 (100%)	0.68 ± 0.63
	61	63	61 (100%)	0.55 ± 0.33
	66	70	66 (100%)	0.83 ± 0.60
2	35	35	35 (100%)	0.41 ± 0.26
	68	70	68 (100%)	0.63 ± 0.64
	77	82	76 (98.7%)	1.40 ± 0.80
3	22	22	21 (95.5%)	0.61 ± 0.19
	44	46	43 (97.7%)	0.72 ± 0.45
	66	71	64 (97.0%)	0.92 ± 0.47

4   Conclusions

A novel method based on Gaussian-blurred images and camera self-calibration process for prostate brachytherapy seed localization using C-arm was described. Gaussian-blurred images are generated from 2-D projection images and are used for tomosynthesis-based 3-D reconstruction. Candidate seeds are extracted and used for correcting the intrinsic camera parameters and the translational pose errors of the images whose pose estimation errors are relatively large. True seed locations are separated from a set of candidate seeds detected from the final reconstruction by solving optimal coverage problem. This method requires a slightly larger number of images compared to the correspondence-based approach, but the attractive feature of the proposed method is that it can recover all the seeds automatically, including the hidden seeds, without an explicit segmentation or a seed correspondence algorithm. In case that the images are acquired with a very small angle separation, the algorithm may have some difficulties in detecting all the true seeds correctly. The relation between the reconstruction and

detection quality and the acquired image angle separation should be further studied. Through various simulations, phantom, and clinical studies, our method was evaluated, successfully localizing the implanted seeds.

References

1. Tubic, D., Zaccarin, A., Beaulieu, L., Pouliot, J.: Automated seed detection and three-dimensional reconstruction, ii. reconstruction of permanent prostate implants using simulated annealing. Med. Phys. 28, 2272–2279 (2001)
2. Narayann, S., Cho, P., Marks, R.: Fast cross-projection algorithm for reconstruction of seeds in prostate brachytherapy. Med. Phys. 29, 1572–1579 (2002)
3. Todor, D.A., Cohen, G.N., Amols, H.I., Zaider, M.: Operator-free, film-based 3d seed reconstruction in brachytherapy. Phys. Med. Biol. 47(12), 2031–2048 (2002)
4. Lam, S.T., Cho, P.S., MarksII, R.J., Narayanan, S.: Three-dimensional seed reconstruction for prostate brachytherapy using hough trajectories. Phys. Med. Biol. 49(4), 557–569 (2004)
5. Jain, A.K., Zhou, Y., Mustafa, T., Burdette, E.C., Chirikjian, G.S., Fichtinger, G.: Matching and reconstructoin of brachytherapy seeds using the hungarian algorithm (MARSHAL). Med. Phys. 32, 3475–3492 (2005)
6. Su, Y., Davis, B.J., Herman, M.G., Robb, R.A.: Prostate brachytherapy seed localization by analysis of multiple projections: Identifying and addressing the seed overlap problem. Med. Phys. 31, 1277–1287 (2004)
7. Singh, V., Mukherjee, L., Xu, J., Hoffmann, K.R., Dinu, P.M., Podgorsak, M.: Brachytherapy seed localization using geometric and linear programming technique. IEEE Trans. Med. Imag. 26, 1291–1304 (2007)
8. Tutar, I.B., Managuli, R., Shamdasani, V., Cho, P.S., Pathak, S.D., Kim, Y.: Tomosynthesis-based localization of radioactive seeds in prostate brachytherapy. Med. Phys. 30, 101–109 (2003)
9. Liu, X., Jain, A.K., Fichtinger, G.: Prostate implant reconstruction with discrete tomography. In: Ayache, N., Ourselin, S., Maeder, A. (eds.) MICCAI 2007, Part I. LNCS, vol. 4791, pp. 734–742. Springer, Heidelberg (2007)
10. Jain, A.K., Mustafa, T., Zhou, Y., Burdette, C., Chirikjian, G.S., Fichtinger, G.: FTRAC - a robust fluoroscope tracking fiducial. Med. Phys. 32, 3185–3198 (2005)
11. Bertsekas, D.P.: Nonlinear programming, 2nd edn. Athena Scientific, Belmont (1999)
12. Lee, J., Liu, X., Jain, A.K., Prince, J.L., Fichtinger, G.: Tomosynthesis-based radioactive seed localization in prostate brachytherapy using modified distance map images. In: Proc. of ISBI, May 2008, pp. 680–683 (2008)